Production Engineering
https://doi.org/10.1007/s11740-023-01242-2

PROCESSES

Surface conditioning of zirconia ceramic by enhanced ultrasonic vibration-assisted burnishing

Toshiki Tsuchida[1] · **Weihai Huang**[1] · **Jiwang Yan**[1]

Received: 31 August 2023 / Accepted: 13 November 2023

Abstract
Yttria-stabilized zirconia (YSZ) ceramic is a widely used material in mechanical and biomedical engineering, such as machine parts and dental implants. For most applications, surface conditioning methods are required to produce smooth and reinforced surfaces with compressive residual stress. This paper investigates the processing characteristics of YSZ under ultrasonic vibration-assisted burnishing (UVB) enhanced by flexible stage and tool rotation techniques, respectively. For the use of flexible stage-enhanced UVB, the fluctuation of burnishing force was greatly reduced. As results, a smooth surface with a roughness of 164 nm Ra was obtained, which shows 39.7% surface roughness reduction from the original surface, and 9.4% surface roughness reduction from the surface burnished with conventional UVB. The burnished surface yielded strong residual compressive stresses of 401 MPa in the burnishing direction and 695 MPa in the step-feed direction. For the use of tool rotation-enhanced UVB, tool rotation-induced arc-shaped surface textures were formed on the burnished surface, and the textures became more distinct and denser as the rotation speed increased. The surface roughness was reduced by 58.9% from the original surface with the tool rotation-enhanced UVB. Stress-induced phase transformation of YSZ was identified in all burnished surfaces. This study demonstrates the feasibility of one-step manufacturing of a smooth surface with high residual compressive stress, which expands the applications of YSZ.

Keywords Zirconia · Ultrasonic vibration-assisted burnishing · Surface conditioning · Surface integrity · Phase transformation

1 Introduction

Yttria-stabilized Zirconia (YSZ) is a kind of promising ceramic material, owing to its excellent biocompatibility and mechanical properties, such as high hardness, fracture toughness, and wear resistance [1, 2]. YSZ exhibits a phenomenon of stress-induced strengthening; as a result, its fracture toughness can be enhanced when subjected to mechanical loading. This mechanism is based on the volume expansion of YSZ during the phase transformation from the tetragonal phase to the monoclinic phase (t-m phase transformation) and is effective in suppressing the extension of cracks on the surface [1]. Due to this unique characteristic, YSZ is applied as an important alternative for conventional metal materials in machine parts and dental implants. However, to replace parts in various applications, the surface quality of the YSZ parts must meet the functional requirements. For example, when the YSZ is applied to dental implants, the surface roughness of less than 200 nm Ra is required to reduce the number of bacteria adhering to the implant surface [3, 4]. Moreover, in applications under cyclic loading conditions, compressive residual stresses need to be applied to the material to improve its fatigue strength and fracture toughness [5]. Although conventional surface finishing methods, such as polishing [6] and diamond cutting [7] can effectively produce a smooth surface on YSZ, they are difficult to induce strong residual compressive stress in the subsurface.

Burnishing is a traditional surface conditioning method widely used in the machining of ductile metallic materials, such as aluminum alloys and stainless steel [8]. It is possible to improve the surface performance, such as surface smoothness, wear resistance, corrosion resistance, and residual compressive stress [9, 10]. In addition, unlike other mechanical machining processes, such as grinding and

✉ Jiwang Yan
yan@mech.keio.ac.jp

[1] Department of Mechanical Engineering, Faculty of Science and Technology, Keio University, Hiyoshi 3-14-1, Kohoku-ku, Yokohama 223-8522, Japan

Published online: 18 December 2023

cutting, which produce a significant amount of chips and can pose environmental issues, burnishing is a non-material removal process known for its environmental friendliness [11]. Recently, micro/nano burnishing has also been attempted to machine toxic brittle materials [12]. In addition, to improve burnishing process, ultrasonic vibration was applied to the tools in burnishing direction or normal to the machining plane to reduce resistance during burnishing [13]. For example, Amanov et al. [14] performed a burnishing process on AZ91D Mg alloy with the tool striking the workpiece surface at a high frequency of 20 kHz. A nanocrystalline surface layer was successfully generated on the top surface, and consequently increased the hardness of the surface compared to that of the bulk material. Teramachi and Yan [15] applied ultrasonic vibration of tool in the burnishing of an additive-manufactured AlSi10 Mg workpiece. They found that the ultrasonic vibration assistance could eliminate a greater number of voids at a greater depth, improve the hardness of workpiece by 24%, and reduced the burnishing force. Ding et al. [16] employed 2D ultrasonic burnishing technology to strengthen the 7075 aluminum alloy surface. After the burnishing, the surface roughness was significantly reduced from micron level (2.490 µm) to nano level (71 nm), meanwhile the hardness was increased from 164 to 252 HV. Moreover, ultrasonic vibration can also be applied to ball/roller burnishing, where sphere/cylinder tools roll on the workpiece surface and the direction of tool vibration is normal to the workpiece surface, to enhance the burnishing performance [17, 18]. However, so far, few studies have focused on the ultrasonic vibration-assisted burnishing (UVB) of brittle materials. Particularly, the processing characteristics of zirconia by UVB is not clear.

When burnishing hard materials, the burnishing force fluctuates sharply with the variation of burnishing depth due to the unevenness of the workpiece surface, which may cause surface fractures of the workpiece and even damages to the burnishing machine and tools. To overcome this problem, in this study, flexible stage-enhanced UVB techniques was proposed for machining YSZ. In this method, the workpiece is fixed on a flexible stage that can move slightly up and down in the loading force direction; thus, during UVB the surface height of the workpiece can be adjusted to keep the burnishing force almost constant via spring compression and extension. This is especially helpful for shape-adaptive finishing of curved surfaces with unevenness. On the other hand, the conventional UVB causes directional distributions of surface roughness and mechanical properties. As a results, surface anisotropy becomes a problem in some applications. To solve this problem, tool rotation was introduced into UVB, where the rotation axis is in the loading force direction. In this way, the tool rotation-induced stirring and grinding effects can improve the uniformity of both the stress distribution and the surface roughness of the workpiece. As these two proposals were motivated for enhancing different aspects of the same UVB process, this paper independently examined the processing characteristics of YSZ under each method, including surface morphology and roughness, residual compressive stress, and phase transformation. The machining mechanisms of the two methods were also clarified. The findings of this study are expected to contribute to the future development of surface conditioning technology of zirconia and other brittle materials.

2 Materials and methods

2.1 Material properties

Fully sintered YSZ plates containing 3 mol% Y_2O_3 for stabilization were used as workpieces. The YSZ materials have ultra-fine grain size in 300–500 nm. The size of the workpieces is 20 × 20 × 2.7 mm. The as-received workpieces have a surface roughness of ~ 275 nm Ra and ~ 3.3 µm Rz. The details of major material properties of YSZ are listed in Table 1.

2.2 Experimental setup for flexible stage-enhanced UVB

Figure 1 shows the flexible stage (Areuse Co., Ltd.) used in this study. The size of the flexible stage is 80 mm × 80 mm × 32 mm. The upper part of the flexible stage is supported by two springs, allowing its movement along the Z-axis, while four cylinders completely restrict its movement in the X-Y plane and any axis of rotation. This mechanism can prevent the titling of the plate and distribute the force evenly to each spring even when the force is not applied at the plate center. The lower part of the flexible stage was mounted on a four-axis (XYZθ) control machine tool (L4S-300 Sodick Co., Ltd.). The YSZ workpiece was fixed on the top of the flexible stage. An ultrasonic vibration spindle unit (Areuse Co., Ltd.) was attached to the Z-axis of the machine tool to drive burnishing tools. The vibration amplitude was set to 2 µm in Z direction. A ball-shaped polycrystalline diamond (PCD) burnishing tool with radius of 1.5 mm (Resmotool Co., Ltd.) was used in the experiments. A S-shaped tool path made of continuous workpiece feeding in Y direction

Table 1 Major material properties of YSZ [19]

Property	Value
Y_2O_3 doping content	3 mol%
Hardness	12.5 GPa
Young's modulus	210 GPa
Fracture toughness	6.0 MPa·$m^{1/2}$

and step feeding in X direction was performed to burnish large areas, as shown in Fig. 2(a). Rough burnishing and fine burnishing were performed by changing the pitch in the step-feeding direction. The rough and fine burnishing tests were performed with the pitches of 50 and 10 µm, respectively. The corresponding burnishing speed (work feed) were 3 and 5 mm/s, respectively. At the initial stage of the burnishing process, the tool gradually approached the workpiece surface in the Z-axis and penetrated the workpiece surface until the force reached 100 N. Then, the workpiece moved along the X and Y axes to begin the burnishing. The experimental conditions of the flexible stage-enhanced ultrasonic vibration burnishing are listed in Table 2.

Table 2 Experimental conditions of flexible stage-enhanced ultrasonic vibration burnishing

Parameters	Values			
Flexible stage	Without		With	
Spring constant [N/mm]	N/A		4.52	
Work feed [mm/s]	3	5	3	5
Pitch [µm/step]	50	10	50	10
Threshold [N]	110			
Initial burnishing force [N]	100			
Vibration frequency [kHz]	27			
Vibration amplitude [µm]	2			
Atmosphere	In lubricating oil			

2.3 Experimental setup for tool rotation-enhanced UVB

The UVB using a rotating tool was conducted with the same machine tool and ultrasonic vibration spindle unit as the UVB using a flexible stage; however, the workpiece was fixed on a rigid stage. During the burnishing process, the tool not only vibrated in Z-direction, but also rotated in X-Y plane, as shown in Fig. 2(b). Several single-path burnishing tests were performed at a constant workpiece feed of 3 mm/s with different rotation speeds. At the initial stage of the burnishing process, like the flexible stage-enhanced UVB, the workpiece started to move until the burnishing force reached to 100 N. The experimental conditions of the rotation-enhanced ultrasonic vibration burnishing are listed in Table 3.

2.4 Measurement and characterization methods

The burnished surfaces were observed by scanning electron microscope (Inspect F50, FEI company). Surface roughness was measured by a laser-probe surface profilometer (MP-3, Mitaka Kohki Co., Ltd). Residual stresses were measured by

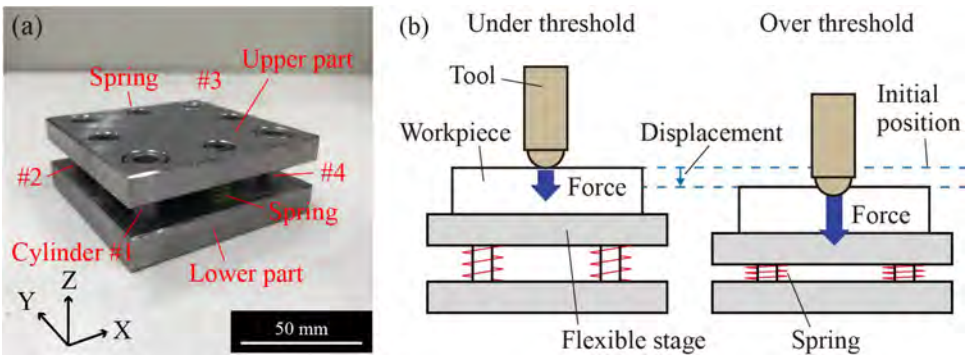

Fig. 1 Flexible stage: **a** photo of appearance; **b** schematic of working principle

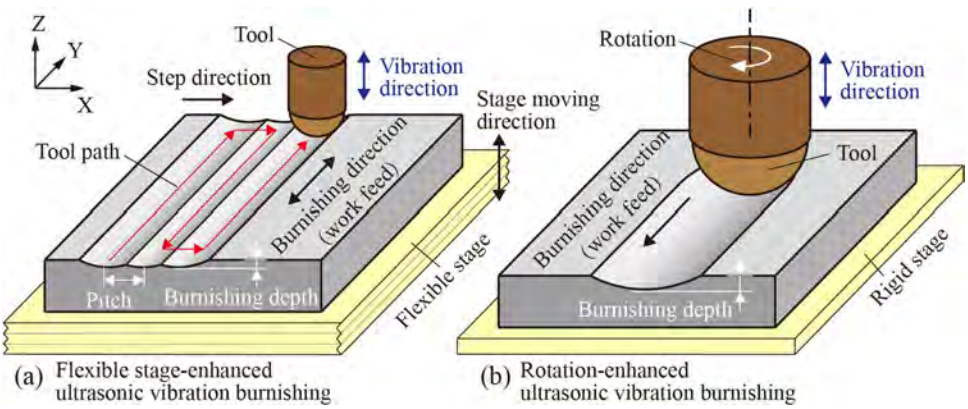

Fig. 2 Schematics of the methods of **a** flexible stage-enhanced ultrasonic vibration burnishing, and **b** rotation-enhanced ultrasonic vibration burnishing. (Not to scale)

a portable residual stress analyzer (μ-X360s, Pulstec Industrial Co., Ltd). Phase transformation was evaluated by X-ray diffraction (D8 Discover, company). During burnishing, a three-component piezoelectric dynamometer (9256C2, Kistler Co., Ltd.) was used to measure the burnishing forces.

3 Results for flexible stage-enhanced UVB

3.1 Surface morphology

The SEM images of the as-received surface and the surfaces finely burnished with and without the flexible stage are shown in Fig. 3. Before burnishing, some protrusions of a few tens of microns can be observed on the surface at low magnification, as shown in Fig. 3(a1). In addition, numerous submicron-scale particles are widely distributed over the entire surface. Figure 3(a2) shows the enlarged view of the surface before burnishing. Ultra-fine grains in the size ranging 300–500 nm and their grain boundary can be clearly observed. After the fine burnishing without the flexible stage, the surface observed at low magnification is shown in Fig. 3(b1). The protrusions and particles were eliminated, and the surface looks much smoother than before burnishing. However, long straight-line marks along the burnishing direction and parallel to each other at the same distance as the pitch of step feed were formed on the burnished surface. In addition, numerous short straight lines along the burnishing direction were formed within the area burnished by one pass. To characterize these short straight lines more clearly, a high-magnification image of an area burnished by one pass was captured, as shown in Fig. 3(b2). It is found that these short straight lines have higher heights relative to their left and right sides of the surfaces, which implies that these lines were formed by extrusion due to the stress concentration around the straight lines. The grain boundaries were completely disappeared on the surface,

Table 3 Experimental conditions of rotation-enhanced ultrasonic vibration burnishing

Parameters	Values
Initial burnishing force [N]	100
Work feed [mm/s]	3
Vibration frequency [kHz]	0, 27
Vibration amplitude [μm]	0, 2
Rotation speed [rpm]	1000, 2000, 4000, 8000
Atmosphere	In lubricating oil

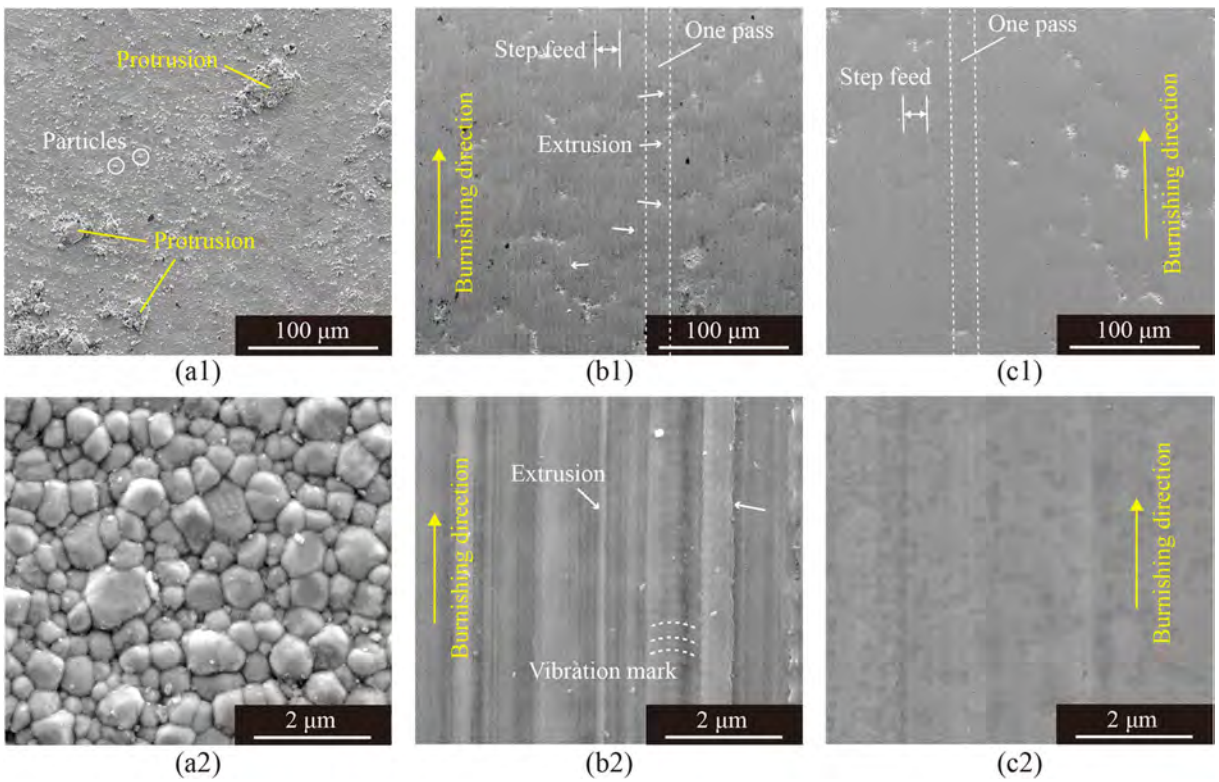

Fig. 3 SEM images of workpiece surfaces: **a** before burnishing, **b** finely burnished without flexible stage, and **c** finely burnished with flexible stage. **a**1–**c**1 are low-magnification images, and **a**2–**c**2 are high-magnification images

but in some area the vibrations marks were formed on the burnished surface. The extrusion and vibration marks on the surface indicate that during the burnishing process without the flexible stage, the contact between the tool and the workpiece was unstable, and thus the distribution of the contact stress was uneven. Figure 3(c1) shows the general view of the surface finely burnished with the flexible stage. The step feed-induced long straight-line marks became less visible, and the short straight-lines marks parallel to the scratching direction were also significantly suppressed. A high-magnification image of an area burnished with the flexible stage was presented in Fig. 3(c2). The burnished surface is very smooth without any extrusion-induced straight-line marks or vibration marks. In addition, it can be noticed that there are many small areas exhibiting different contrast on the surface, which corresponds to different grains. However, the density of grain boundaries was reduced owing to the plastic deformation of the grains. The grain boundaries on the surface with the flexible stage were not completely disappeared like those on the surface without the flexible stage, which may be attributed to the fact that the actual burnishing force with the flexible stage is smaller that without the flexible stage. This issue will be discussed in Sect. 3.5.

The appearances of the workpiece surfaces burnished with and without the flexible stage are compared with the as-received workpiece surface, as shown in Fig. 4. All samples were placed on a patterned table. Owing to the rough surface of the as-received workpiece, it is difficult to mirror the pattern of the table. In contrast, the surfaces burnished with and without the flexible stage are smooth, leading to a specular reflection; as a result, the reflection of the table's pattern in the burnished surfaces can be observed. However, the exact difference between surfaces burnished with and without the flexible stage is hard to distinguish from the photos. The surface roughness will be quantitatively discussed in Sect. 3.2.

3.2 Surface roughness

To evaluate the roughness of the burnished surfaces, surface profiles along the burnishing direction were measured on the sample burnished with and without the flexible stage, and compared to the surface profile of the as-received sample, as shown in Fig. 5. Large fluctuation (peak-to-valley of 0.2–3.5 μm) relative to the averaged surface was obtained in the surface profile of the as-received workpiece. Sharp peaks and deep valleys were observed in Fig. 5(a), which may be caused by the protrusions and craters on the as-received workpiece surface, respectively. After the burnishing without the flexible stage, the variation of the profile of the burnished surface was

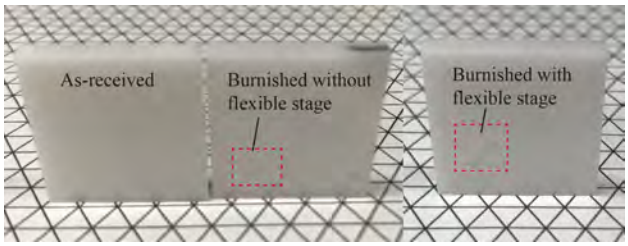

Fig. 4 Comparison of the appearance of the surface burnished with/without flexible stage and the as-received surface

reduced to 0–1.6 μm. Additionally, peaks had a moderate sharpness, and the valleys became shallow, as shown in Fig. 5(b). This implies that part of the protruding material was pressed and flowed to fill the craters; as a result, the burnished surface became relatively smooth. In contrast, after the burnishing with the flexible stage, the variation of the profile of the burnished surface was to 0.1–1.4 μm, as shown in Fig. 5(c), which was slightly smaller than that of the burnished surface without the flexible stage. Moreover, the protrusions-induced peaks became blunt. This indicates that the protruding material was compered more with the assistance of the flexible stage, due to more stable contact stress.

The arithmetic mean roughness of the as-received surface and the burnished surfaces with/without the flexible stage measured along the burnishing and step feed directions were calculated, as shown in Fig. 6. Under the conditions without the flexible stage, the arithmetic mean roughness was reduced by 33.6% in the burnishing direction and by 36.1% in the step feed direction. In contrast, under the conditions with the flexible stage, the arithmetic mean roughness was reduced by 39.8% in the burnishing direction and by 39.2% in the step feed direction. Additionally, it is worth noting that ultrasonic vibration-assisted burnishing process can produce a surface with roughness below the threshold required for use as a dental material (200 nm Ra). Therefore, burnishing process is a promising replacement for polishing process. The influence of the pitch of the step feed was not included in this figure. It will be systematically investigated in the next step when considering surface functions.

3.3 Residual compressive stress

The residual compressive stress of the burnished surface with/without the flexible stage along the burnishing and step feed directions were measured and compared with that of the surface by polishing, which is a conventional finishing process of YSZ. The residual compressive stress of the polished surface is 17 MPa, as shown in Fig. 7. After the burnishing with/without the flexible stage, the residual compressive stresses of the surface were greatly increased,

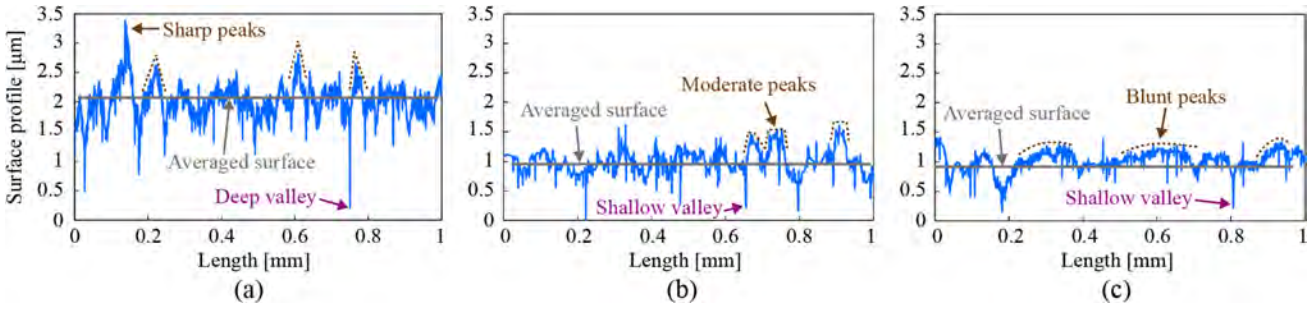

Fig. 5 Surface profiles of the workpieces: **a** as-received, **b** burnished without flexible stage, and **c** burnished with flexible stage

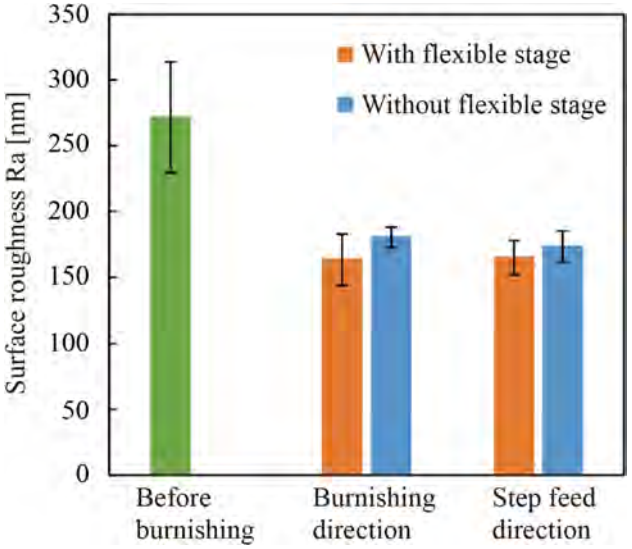

Fig. 6 Comparison of the arithmetic mean roughness of the as-received surface and the surfaces burnished with/without flexible stage measured along different directions

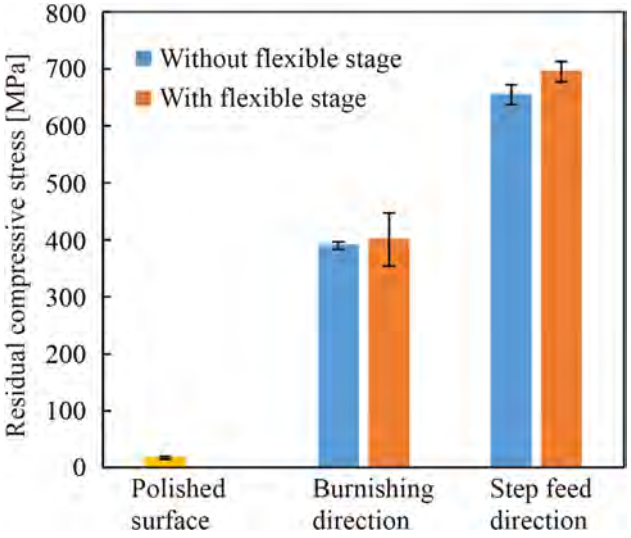

Fig. 7 Comparison of the residual compressive stress of the as-received surface and the surfaces burnished with/without flexible stage measured along different directions

and the residual compressive stress induced by the flexible stage-assisted burnishing is slightly higher than that by without the flexible stage-assisted burnishing, which has the stress of 401 MPa in the burnishing direction and 695 MPa in the step feed direction. This indicates that the residual compressive stress in the burnishing and step feed directions induced by the flexible stage-assisted burnishing is 22 times and 41 times higher than that of the polished surface, respectively. This stress is expected to improve the fracture toughness and enhance fatigue strength of YSZ [5, 20].

It is important to note that the distribution of the residual compressive stress appeared to be distinct different along different directions after the burnishing. Particularly, the stress was much larger in the step feed direction than in the burnishing direction, regardless the use of flexible stage or not. Such stress distribution has also been reported in the grinding of YSZ [6]. This is because in the burnishing direction, the compressive action was only performed on the material in front of the tool which has not yet been deformed; while in the step feed direction, side of the material to be burnished in current tool path has been compressed by the previous tool path, as illustrated in Fig. 8. As a result, in the step feed direction a stronger plastic deformation was produced between the two paths by bidirectional compressive stress, causing a much larger residual compressive stress.

3.4 Phase transformation

In general, YSZ is stable as a tetragonal phase at room temperature, but under stress, it undergoes tetragonal to monoclinic (t-m) phase transformation. Therefore, the possible transformation in the burnished surfaces with/without the flexible stage was evaluated by XRD. Their XRD spectra are plotted together with the spectrum of the as-received surface, as shown in Fig. 9. In the XRD spectrum

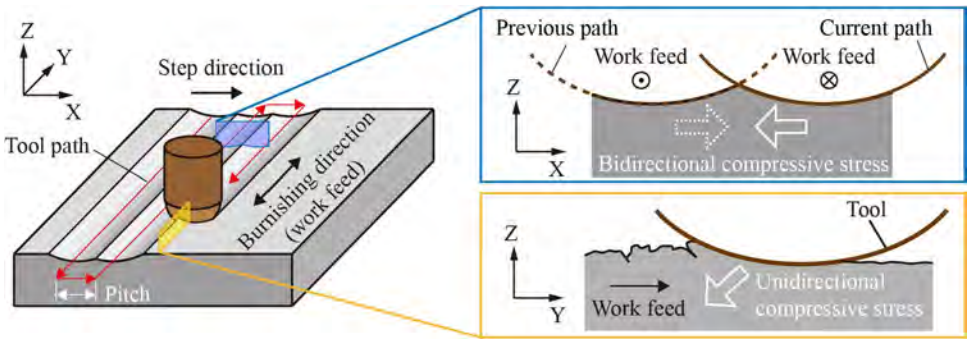

Fig. 8 Schematic model of the formation of residual compressive stress in various directions. (Not to scale)

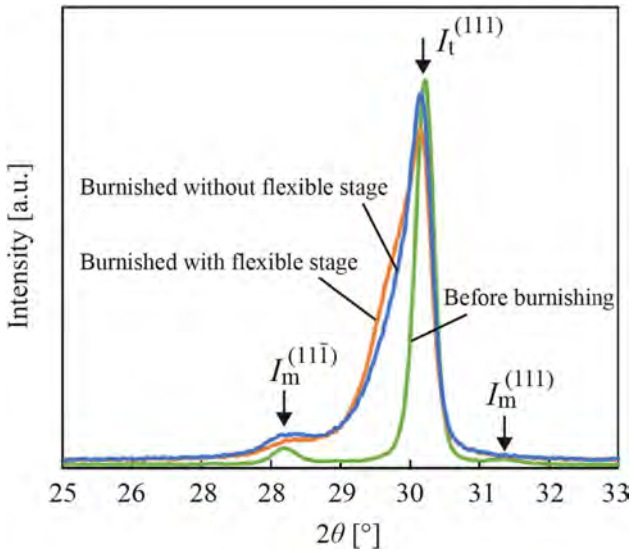

Fig. 9 Comparison of the XRD spectra of the as-received surface and the surfaces burnished with/without flexible stage

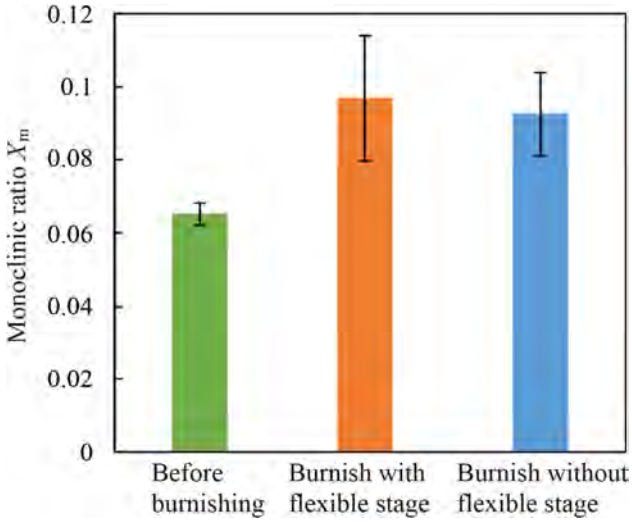

Fig. 10 Comparison of the monoclinic ratio of the as-received surface and the surfaces burnished with/without flexible stage

of the as-received surface, a sharp peak $I_t^{(111)}$ at $2\theta = 30°$ corresponding to tetragonal phase (111) was observed, and two small peaks $I_m^{(11-1)}$ and $I_m^{(111)}$ at $2\theta = 28°$ and 31.2° corresponding to monoclinic phase (11−1) and (111) also appeared. After burnishing, the intensity of the main peak $I_t^{(111)}$ became weaker and broader, meanwhile, the peak $I_m^{(111)}$ disappeared due to the broadening of the $I_t^{(111)}$ peak, which are caused by burnishing-induced plastic deformation of the crystal lattice.

To quantitatively evaluate t-m phase transformation, the monoclinic ratio X_m based on XRD spectrum was calculated using the following Eqs. [21, 22]:

$$X_m = \frac{I_m^{(111)} + I_m^{(11-1)}}{I_m^{(111)} + I_m^{(11-1)} + I_t^{(111)}} \quad (1)$$

The calculated monoclinic ratios of different samples are shown in Fig. 10. Compared to the monoclinic ratio of the as-received surface, the monoclinic ratio of the burnished surface with and without the flexible stage increased by 48.7% and 42.0%, respectively. Nevertheless, the monoclinic ratios in both cases are less than 0.1, and the tetragonal phase, which is necessary for the strengthening mechanism of the stress-induced phase transformation, still plays a dominant role. The monoclinic ratio was kept below 0.1 after burnishing is thought to be that the burnishing-induced compressive stress increased the energy required for phase transformation with volume expansion, which makes it difficult for phase transformation to occur further [23].

3.5 Mechanisms of UVB with a flexible stage

The burnishing force normal to the workpiece surface is measured at both rough and fine burnishing conditions, as plotted in Fig. 11(a) and (b). Owing to the fact that a S-shaped tool path was performed to burnish a large area, as illustrated in Fig. 11(c), and the workpiece surface was slightly tilted relative to the X-Y plane of the machine tool, the burnishing force was gradually increased from the side with a lower Z-position to the side with a higher Z-position

as the tool moved forward. Subsequently, after a step feed was performed, the burnishing force started to decrease from the side with a higher Z-position to the side with a lower Z-position as the tool moved back. As a result, a wave-like curve of cutting force was formed throughout the burnishing process. All measured burnishing forces have a minimum value of 100 N, which matches the preset initial burnishing force, while the average forces fluctuate around 130 N due to the tilted workpiece surface. Besides, it can be clearly seen that the fluctuation range of the forces in rough and fine burnishing are significantly reduced with the use of the flexible stage than without it. Specifically, the burnishing force was reduced up to 95.4% and 97.7% in the rough and fine burnishing, respectively.

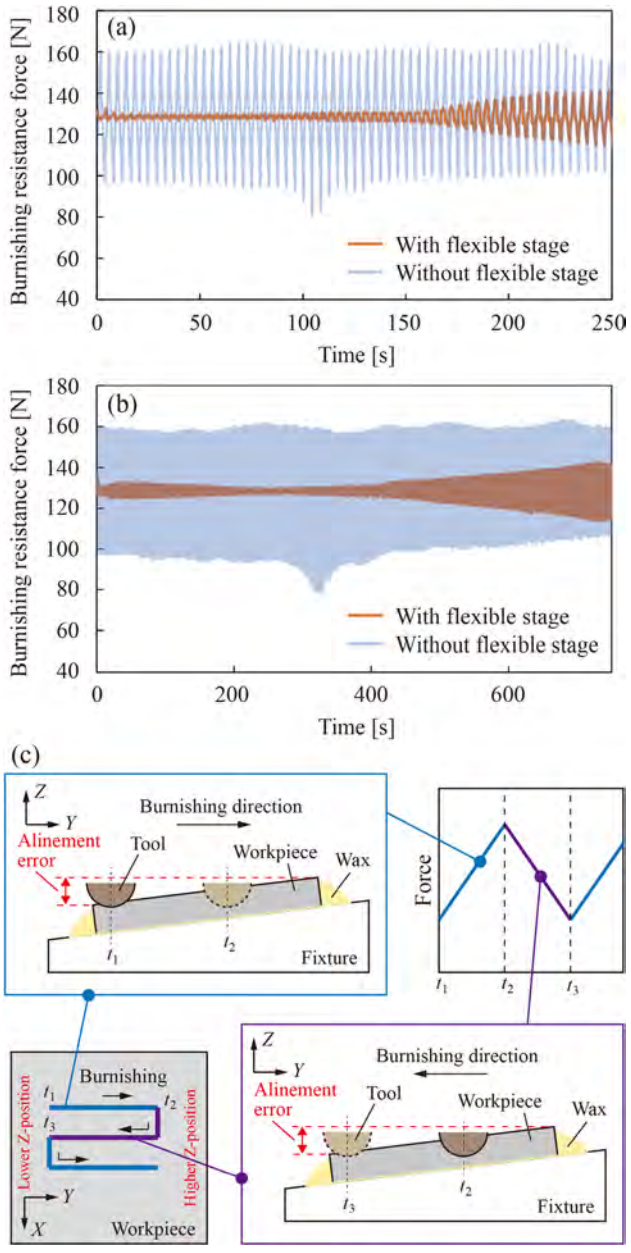

Fig. 11 Comparison of the burnishing resistance with and without flexible stage assistance: **a** under rough burnishing (burnishing speed of 3 mm/s and pitch of 50 μm), **b** under fine burnishing (burnishing speed of 5 mm/s and pitch of 10 μm). **c** Schematic of the mechanisms of burnishing force fluctuation

To reveal the mechanism of the reduction of the burnishing force fluctuation, a schematic model of the machining process is illustrated in Fig. 12. For simplicity, the flexible stage is represented by a spring, whose spring constant is k. When the tool is located at an initial position, the spring is compressed by a length of l. Therefore, according to the Hooke's law, the burnishing force at the initial position can be calculated by following equation:

$$F_{B0} = kl \tag{2}$$

Due to the unevenness of the original workpiece surface, spring (flexible stage) will move up and down as the workpiece is fed. When the tool is located at a hill portion of the workpiece surface, as shown in Fig. 12(a), the displacement of the spring is δ_1 in the compressive direction; whereas when the tool is located in a valley portion of the workpiece surface, as shown in Fig. 12(b), the displacement of the spring is δ_2 in the tension direction. Thus, the burnishing force at the hill and valley positions can be expressed by Eqs. (3) and (4), respectively.

$$F_{B1} = k(l + \delta_1) \tag{3}$$

$$F_{B2} = k(l - \delta_2) \tag{4}$$

According to Newton's third law of motion, the resistance force R_B measured by dynamometer should be equal to the burnishing force F_B. Therefore, the fluctuation value of the burnishing force can be given by:

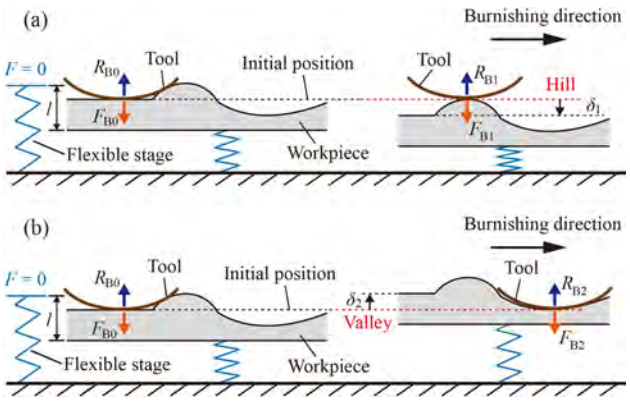

Fig. 12 Schematic models of the burnishing process with flexible stage when the tool is located at **a** hill, and **b** valley portions of the workpiece surface

$$\Delta R_{\mathrm{B}} = \pm k\delta \tag{5}$$

where δ is the absolute value of the displacement of the current position relative to the initial position. The formula has positive sign when the spring is compressed and has negative sign when the spring is extended relative to the initial position.

When burnishing the workpiece without the flexible stage, it can be regarded as replacing the spring with a stage made of workpiece material; consequently, the equivalent spring constant of the stage made of workpiece material is equal to the hardness of the workpiece. As the spring constant k is much smaller than hardness of the workpiece, the fluctuation range of the burnishing force with the flexible stage is much smaller than that without the flexible stage. The smaller fluctuation range of the force indicates that a sudden change of the burnishing force was suppressed. As a result, the use of a flexible stage can inhibit crack formation and then create smooth surfaces. Moreover, the flexible stage is considered to be effective when burnishing workpieces with three-dimensional surfaces, because it can prevent damages from geometric irregularities such as protrusions.

4 Results for tool rotation-enhanced UVB

4.1 Surface morphology

The SEM images of the surface burnished with and without ultrasonic vibration under different tool rotation speeds are shown in Fig. 13. In general, the surfaces burnished with/without vibration shows similar surface features. When the tool rotation speed was more than 4000 rpm, the tool rotation-induced periodic surface texture was evident and became dense as the tool rotation speed increased. However, when the tool rotation speed was less than 2000 rpm, numerous fine curved lines appeared on the surface, which makes it difficult to distinguish the periodic surface texture, especially when the tool rotation speed decreased to 1000 rpm. The formation of the periodic surface texture will be discussed in Sect. 4.4.

To further characterize the fine curved lines on the burnished surface, high-magnification SEM image of the surface at each condition was observed, as shown in Fig. 14. At the low tool rotation speed (< 2000 rpm), uneven extrusions perpendicular to the burnishing direction occurred on the surface, which is caused by the rotary motion of the tool. These rotation-induced extrusions are more pronounced than the step feed-induced extrusions with a non-rotating tool (see Fig. 3); as a result, burrs were formed on the surface. In addition, on the surface burnished without vibration, blurred grain boundaries can be observed. However, the quality of the surface burnished with vibration is worse than that without vibration, due to the vibration marks additionally formed on the surface. At the high tool rotation speed (> 4000 rpm), the occurrence of the rotation-induced uneven extrusions was significant suppressed as the tool rotation speed increased, especially when vibration was applied. As the vibration marks were disappeared, the quality of the

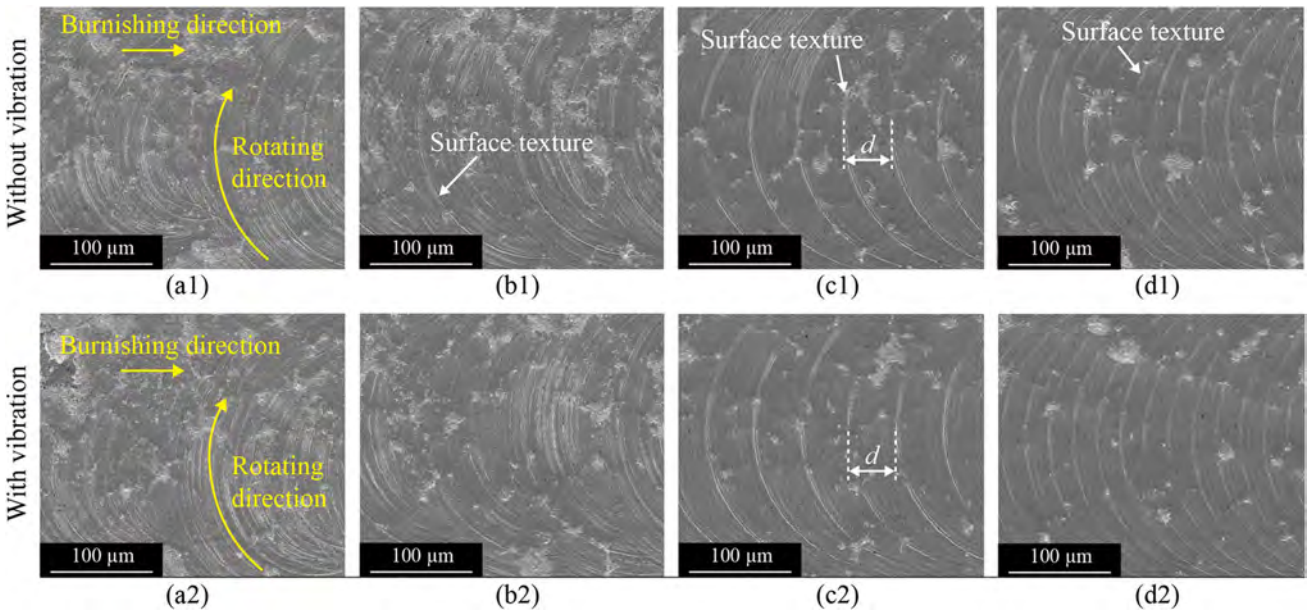

Fig. 13 SEM images of the burnished surface by a rotation tool at **a** 1000 rpm, **b** 2000 rpm, **c** 4000 rpm, **d** 8000 rpm. **a**1–**d**1 are produced without ultrasonic vibration, **a**2–**d**2 are produced with ultrasonic vibration

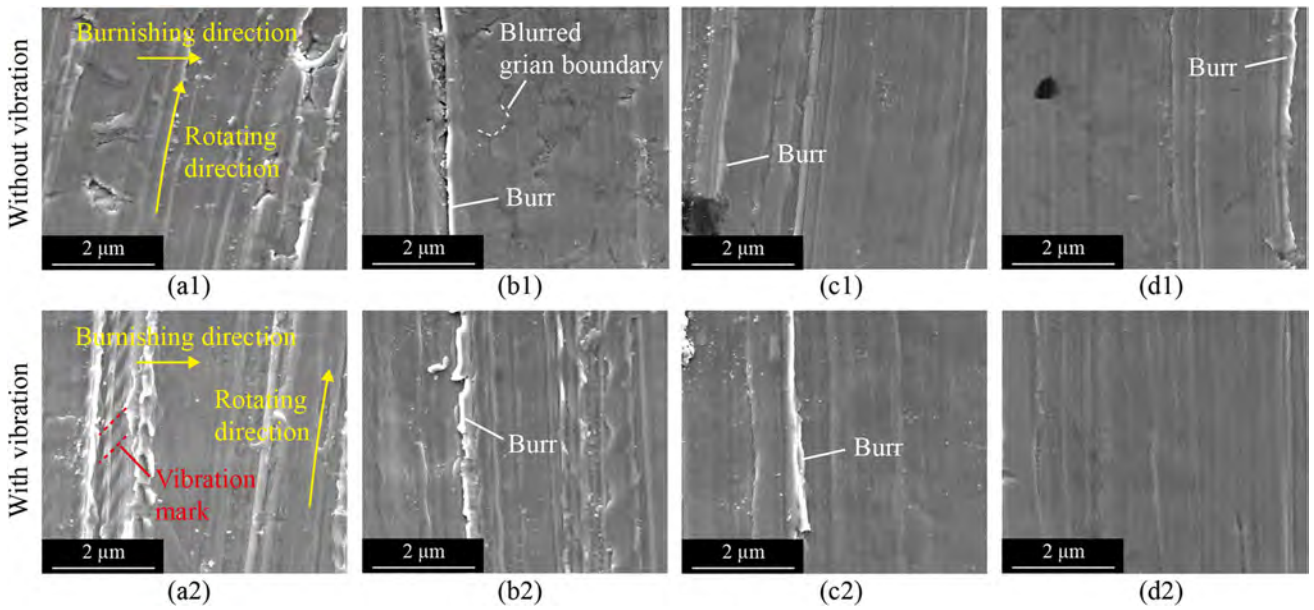

Fig. 14 Enlarged SEM images of the burnished surface by a rotation tool at **a** 1000 rpm, **b** 2000 rpm, **c** 4000 rpm, **d** 8000 rpm. **a**1–**d**1 are produced without ultrasonic vibration, **a**2–**d**2 are produced with ultrasonic vibration

surface burnished with vibration becomes better than that without vibration, at the high tool rotation speed.

4.2 Surface roughness

The roughness of the as-received surface and the surfaces burnished with and without vibration at different tool rotation speeds were evaluated, as shown in Fig. 15. Obviously, the roughness of all burnished surfaces is significantly reduced compared to the as-received surface. Moreover, the burnished surfaces became smoother as the rotational speed increased. Particularly, the ultrasonic vibration burnishing with a rotating tool of 8000 rpm rotation speed reduced the surface roughness by 58.9% compared to the as-received surface. However, at low tool rotation speed (< 2000 rpm) the surface roughness produced by vibration burnishing is worse than that by the burnishing without vibration. At high tool rotation speed (> 4000 rpm), the vibration burnishing generated a better surface finish than the burnishing without vibration. The results of surface roughness are consistent with the observation of surface morphology shown in Figs. 13 and 14.

A more uniform plastic deformation of the material is occurred at a higher tool rotation speed. This is supposed to be caused by the fact that when the tool rotation speed increases, the number of times that each region is subjected to rotary burnishing will increase. To quantify the relationship between the number of burnishing times of a certain region and the tool rotation speed, a kinematic model of the burnishing process with tool rotation was developed, as

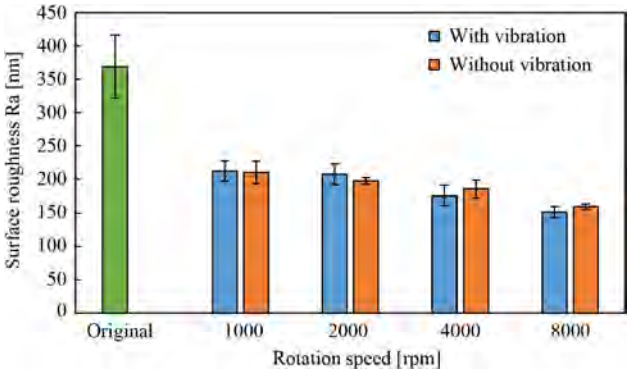

Fig. 15 Comparison of the arithmetic mean roughness of the surfaces burnished with/without vibration at different tool rotation speed

shown in Fig. 16. The number of rotation times of tool (n) during the period from the first time the tool contacts the red point to the last time the tool contacts the red point can be calculated by the following equation:

$$n = \frac{2Nr}{60v_b} + 1 \tag{6}$$

where N is the tool rotation speed, v_b is the burnishing speed (also the work feed speed), and r is the contact radius between the tool and workpiece. Thus, the number of burnishing times for a certain region at the tool rotation speed of 1000, 2000, 4000, and 8000 rpm, are 2.2, 4.4, 8.9 and 17.8, respectively. Therefore, when the tool rotates at a large speed to burnish the

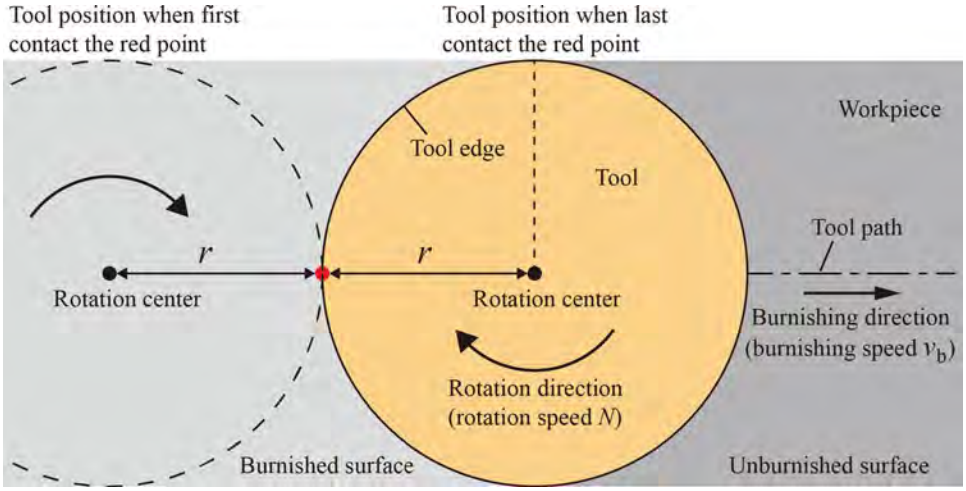

Fig. 16 Kinematic model of the burnishing process with tool rotation

material, the burrs formed in the beginning of burnishing will be gradually smoothed out by subsequent burnishing. Besides, the benefits of vibration burnishing in smoothing workpiece surfaces also become less apparent when tool rotation is applied, because the workpiece can be burnished multiple times with a rotating tool even vibration is not applied to the tool.

4.3 Phase transformation

When the tool is rotating during the burnishing, the linear velocity of an arbitrary contact point varies with its distance from the center of tool rotation. Thus, the state of machining may be changing along the direction perpendicular to the burnishing direction, that is, the center and the edge of the burnished groove may undergo different degrees of microstructural changes. To confirm this, the Raman spectra of the edge and center regions of the surface under ultrasonic vibration burnishing with a rotating tool of different rotation speeds are characterized. For example, Fig. 17(a) shows a microscope image of a groove under ultrasonic vibration burnishing with a rotating tool of 1000 rpm. The Raman measurements were performed in the center and edge regions indicated in Fig. 17(a), and the corresponding Raman spectra are plotted in Fig. 17(b). For both spectra, main peaks at the wavenumber of 145 cm^{-1} and 265 cm^{-1} were observed, indicating that the tetragonal phase are dominant. While the presence of monoclinic phase was also confirmed, which proved by the peaks at 181 cm^{-1} and 190 cm^{-1}. To quantify the t-m phase transformation of the center and edge regions at different burnishing conditions, monoclinic ratio of each region and condition was calculated according to the following equation, and compared with the as-received workpiece.

$$V_m = \frac{I_m^{(181)} + I_m^{(190)}}{2.07I_t^{(147)} + I_m^{(181)} + I_m^{(190)}} \quad (7)$$

where V_m is the monoclinic ratio calculated by Raman spectrum, $I_m^{(181)}$ and $I_m^{(190)}$ are the integrated intensity of the monoclinic peak at 181 cm^{-1} and 190 cm^{-1}, respectively. $I_t^{(147)}$ is the integrated intensity of the tetragonal peak at 147 cm^{-1}.

Figure 18(a) and (b) present the monoclinic ratio of the burnished surface under vibration and non-vibration conditions. For both conditions, the monoclinic ratio at the edge region tends to have a larger value than that at the center region. This may be due to the fact that the relative velocity between the tool and workpiece surface increased with the distance from the tool rotation center to the tool-workpiece contact point, which leads to a stronger the shear component of the force applied to the material. Compared with the original value, for the monoclinic ratio of the edge region, the surfaces by non-vibration burnishing tend to have a smaller value at each tool rotation speed, while the surfaces by vibration burnishing have a greater value when the tool rotation speed is low (< 2000 rpm), and have a sudden decrease when the tool rotation speed is high (> 4000 rpm). For the monoclinic ratio of the center region, each burnishing conditions produced a lower value than the original surface. This indicates that the t-m phase transformation at the center region was suppressed during the tool rotating burnishing, regardless the assistance of ultrasonic vibration, because a large burnishing depth at the center region caused compressive stress to dominate [19].

4.4 Mechanisms of UVB with a rotating tool

The surface burnished with a rotating tool has a periodic surface texture along the burnishing direction (see Fig. 13), which is different from the surface burnished without a rotating tool (see Fig. 3). To understand the formation mechanism of the periodic surface texture, kinematic analysis of the rotating tool was performed, and the trajectory of the tool

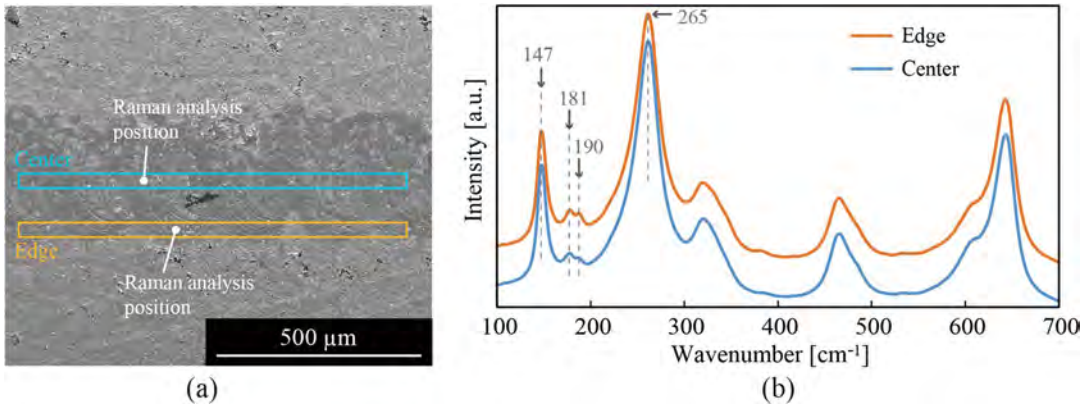

Fig. 17 **a** Microscope image, and **b** Raman spectra of the edge and center regions of the surface under ultrasonic vibration burnishing with a rotating tool of 1000 rpm

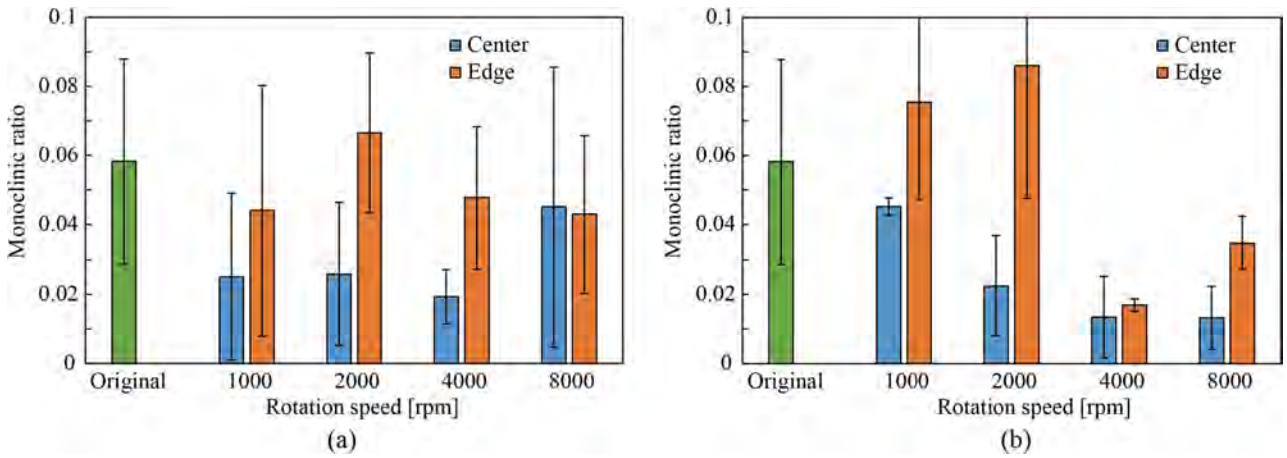

Fig. 18 Comparison of the monoclinic ratio of the burnished surface with different tool rotation speeds when **a** ultrasonic vibration is not applied, and **b** ultrasonic vibration is applied

edge in tool rotation burnishing is schematically shown in Fig. 19. If the tool only rotates without linear motion relative to the workpiece, for a certain point P', its trajectory on the workpiece is a circle whose radius, r, is equal to the distance from the point to the rotation center. Thus, the trajectory of P' can be expressed by the following equations:

$$P'_x(t) = r(1 + \cos(\omega t - \pi)) \tag{8}$$

$$P'_y(t) = -r \sin(\omega t - \pi) \tag{9}$$

where t is the time, ω is the angular velocity of the tool rotation and equal to $2\pi N$.

When the tool starts to rotate and linearly move relative to the workpiece along the positive direction of x-axis with a speed of v_b, for a point P' located at the same location as P', its y-coordinate is the same as the y-coordinate of point, because the motion state in the direction

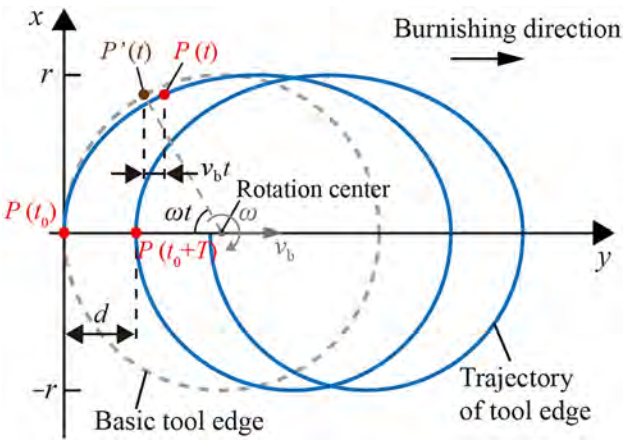

Fig. 19 Schematic of the trajectory of the tool edge in tool rotation burnishing

of y-axis is the same. However, the x-coordinate of point P has a displacement space of $v_b t$ with respect to point P', as shown in Fig. 19, owing to the movement of the tool along the direction of x-axis. Thus, the trajectory of point P can be expressed by the following equations:

$$P_x(t) = P_x'(t) + v_b t \tag{10}$$

$$P_y(t) = P_y'(t) \tag{11}$$

During the burnished with a rotating tool, material extrusion would occur at the edge of the tool-workpiece contact area, thus the extruded material follows the trajectory described by Eqs. (10) and (11) forming the periodic surface texture. In addition, the pitch distance of the periodic surface texture d can be calculated by:

$$d = v_b T \tag{12}$$

where T is the time for one revolution of the tool.

When the tool rotation speed of 4000 and 8000 rpm, T are 0.015 and 0.0075 s, respectively. Substituting the value of T into Eq. (12), the calculated d at the tool rotation speed of 4000 and 8000 rpm are 45 and 22.5 μm, respectively. The actual d was measured by averaging all pitch distances in the observation area of Fig. 13(c) and (d), and compared with the theoretical value, as plotted in Fig. 20. The pitch distance of the periodic surface texture produced during ultrasonic vibration burnishing matches well with the theoretical values under various tool rotation speed. However, the pitch distance caused by non-ultrasonic vibration burnishing is 11.3% larger than by ultrasonic vibration burnishing at 4000 rpm tool rotation speed, and 12.1% larger at 8000 rpm tool rotation speed. This indicates that the machining state under vibration burnishing is approaching more closely to the theoretical state, which is good for controlling the machining process. The deviation of d under non-vibration burnishing may be caused by an unstable contact of the tool and workpiece.

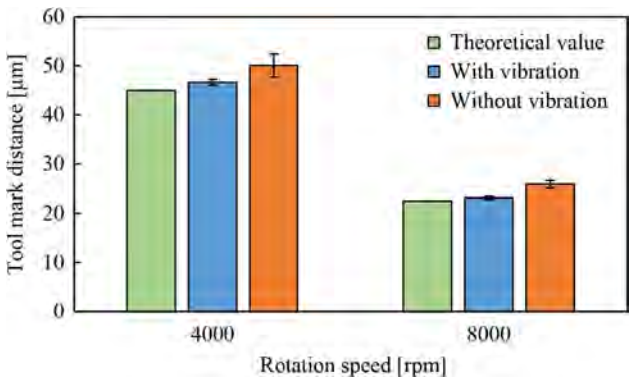

Fig. 20 Comparison of theoretical and measured distance of tool rotation-induced burnishing marks

5 Conclusion

In this study, ultrasonic vibration-assisted burnishing using a flexible workpiece stage and a rotating tool were performed on Yttria-stabilized Zirconia (YSZ) for surface conditioning. The processing characteristics, including surface morphology, surface roughness, residual compressive stress, and phase transformation, were examined. The mechanisms of these ultrasonic vibration-assisted burnishing methods were discussed. The main conclusions are as follow:

- Ultrasonic vibration-assisted burnishing is an effective method to improve surface quality. When burnishing using a flexible workpiece stage, the fluctuation of burnishing force can be greatly reduced (up to 97.7%), leading to a better surface roughness. A smooth surface with a roughness of 164 nm Ra was obtained with using a flexible workpiece stage, which shows 39.7% surface roughness reduction over the original surface, and 9.4% surface roughness reduction over the surface burnished without using a flexible workpiece stage.
- In a large area created by the combination of continuous burnishing motion and step feed motion, the residual compressive stress along the step-feed direction of 695 MPa is much larger than that along the burnishing direction of 401 MPa, because the material underwent bidirectional compression along the step-feed direction.
- When burnishing using a rotating tool, the surface quality can also be improved. However, at low rotation speeds (< 2000 rpm), vibration burnishing caused higher surface roughness than non-vibration burnishing; while at high rotation speeds (> 2000 rpm), vibration burnishing caused lower surface roughness than non-vibration burnishing. This is because the number of times that each region is subjected to rotary burnishing will increase as the rotation speed, eliminating vibration marks.
- Arc-shaped surface textures were formed on the burnished surface due to the tool rotation, and the textures became more distinct and denser as the rotation speed increased. The surface roughness under tool rotation burnishing was reduced by 58.9% over the original surface.
- Stress-induced phase transformation of YSZ was identified in all burnished surfaces. When burnishing using a flexible workpiece stage, the tetragonal phase in the as-received workpiece tends to transform into the monoclinic phase. However, when burnishing using a rotating tool, the trend of phase transformation highly depends on the location of the tool workpiece contact. At the center

of the burnished area, the monoclinic phase was reduced, whereas at the edge of the burnished area, the monoclinic phase increased compared to the as-received workpiece.

The reduction of surface roughness and the adding of residual compressive stress on YSZ were achieved simultaneously by enhanced ultrasonic vibration-assisted burnishing. This study might provide a potential alternative to surface smoothing of YSZ and serves as reference for shape-adaptive surface conditioning of various materials. Flexible stage-enhanced UVB significantly reduces the burnishing force during area burnishing, accompanied by t-m phase transformation. In contrast, tool rotation-enhanced UVB suppresses t-m phase transformation. As these two proposals were motivated for enhancing different aspects of the same UVB process, their effects are investigated independently in this paper. However, the integration of the two methods is expected to be more effective. The synthetic effects of the integration of these methods in the UVB will be further investigated in the future.

Acknowledgements The authors thanks Areuse Co., Ltd. and Pulstec Industrial Co., Ltd. for providing technical supports.

Declarations

Conflict of interest The authors declare that they have no conflict of interest.

References

1. Garvie RC, Hannink RH, Pascoe RT (1975) Ceramic steel? Nature 258(5537):703–704
2. Soon G, Pingguan-Murphy B, Lai KW, Akbar SA (2016) Review of zirconia-based bioceramic: surface modification and cellular response. Ceram Int 42(11):12543–12555
3. Yin L, Nakanishi Y, Alao A, Song X, Abduo J, Zhang Y (2017) A review of engineered zirconia surfaces in biomedical applications. Proc CIRP 65:284–290
4. Lu A, Gao Y, Jin T, Luo X, Zeng Q, Shang Z (2020) Effects of surface roughness and texture on the bacterial adhesion on the bearing surface of bio-ceramic joint implants: an in vitro study. Ceram Int 46(5):6550–6559
5. Takahashi K, Iwanaka K, Koike H (2017) Increased fatigue strength of partially stabilised zirconia achieved by shot peening. Mater Sci Technol 33(5):623–628
6. Minguela J, Slawik S, Mücklich F, Ginebra MP, Llanes L, Mas-Moruno C, Roa JJ (2020) Evolution of microstructure and residual stresses in gradually ground/polished 3Y-TZP. J Eur Ceram Soc 40(4):1582–1591
7. Yan J, Okuuchi T (2019) Chip morphology and surface integrity in ultraprecision cutting of yttria-stabilized tetragonal zirconia polycrystal. CIRP Ann 68(1):53–56
8. Mahajan D, Tajane R (2013) A review on ball burnishing process. Int J Sci Res 3:1–8
9. Li FL, Xia W, Zhou ZY, Zhao J, Tang ZQ (2012) Analytical prediction and experimental verification of surface roughness during the burnishing process. Int J Mach Tools Manuf 62:67–75
10. Raza A, Kumar S (2022) A critical review of tool design in burnishing process. Tribol Int 174:107717
11. Huang W, Yan J (2023) Effect of tool geometry on ultraprecision machining of soft-brittle materials: a comprehensive review. Int J Extreme Manuf 5(1):012003
12. Huang W, Yan J (2021) Chip-free surface patterning of toxic brittle polycrystalline materials through micro/nanoscale burnishing. Int J Mach Tools Manuf 162:103688
13. Kumar VC, Hutchings IM (2004) Reduction of the sliding friction of metals by the application of longitudinal or transverse ultrasonic vibration. Tribol Int 37(10):833–840
14. Amanov A, Penkov OV, Pyun Y, Kim D (2012) Effects of ultrasonic nanocrystalline surface modification on the tribological properties of AZ91D magnesium alloy. Tribol Int 54:106–113
15. Teramachi A, Yan J (2019) Improving the surface integrity of additive-manufactured metal parts by ultrasonic vibration-assisted burnishing. J Micro Nano-Manuf 7(2):021001
16. Ding C, Feng S, Qiao Z, Zhou Z, Piao Z (2023) Running-in performance of 7075 aluminum alloy strengthened by burnishing technology. J Mech Sci Technol 37(5):2545–2553
17. Zhao J, Liu Z (2020) Plastic flow behavior for machined surface material Ti-6Al-4V with rotary ultrasonic burnishing. J Mater Res Technol 9(2):2387–2401
18. Travieso-Rodríguez JA, Jerez-Mesa R, Gómez-Gras G, Llumà-Fuentes J, Casadesús-Farràs O, Madueño-Guerrero M (2019) Hardening effect and fatigue behavior enhancement through ball burnishing on AISI 1038. J Mater Res Technol 8(6):5639–5646
19. Kosai K, Yan J (2020) Effects of cyclic loading on subsurface microstructural changes of zirconia polycrystals in nanoscale mechanical processing. Int J Mach Tools Manuf 159:103626
20. Takahashi K, Iwanaka K, Osada T, Koike H (2015) Increase in strength of partially stabilized zirconia after shot peening. J Mater Eng Perform 24(9):3573–3578
21. Zhuang Y, Zhu Z, Jiao T, Sun J (2019) Effect of aging time and thickness on low-temperature degradation of dental zirconia. J Prosthodont 28(1):e404–e410
22. Liu E, Xiao G, Jia W, Shu X, Yang X, Wang Y (2017) Strain-induced phase transformation behavior of stabilized zirconia ceramics studied via nanoindentation. J Mech Behav Biomed Mater 75:14–19
23. Muñoz-Tabares JA, Jiménez-Piqué E, Reyes-Gasga J, Anglada M (2011) Microstructural changes in ground 3Y-TZP and their effect on mechanical properties. Acta Mater 59(17):6670–6683